ESC European Society of Cardiology

Cardiovascular Research (2024) **120**, 630–643
https://doi.org/10.1093/cvr/cvae014

Histone demethylase KDM5 regulates cardiomyocyte maturation by promoting fatty acid oxidation, oxidative phosphorylation, and myofibrillar organization

Manisha Deogharia [1], Leslye Venegas-Zamora[2], Akanksha Agrawal [2], Miusi Shi [3], Abhinav K. Jain[4], Kevin J. McHugh [3,5], Francisco Altamirano [2,6], Ali J. Marian[1], and Priyatansh Gurha [1]*

[1]Center for Cardiovascular Genetics, Institute of Molecular Medicine, University of Texas Health Sciences Center at Houston, 6770 Bertner Street, C950G, Houston, TX 77030, USA; [2]Department of Cardiovascular Sciences, Houston Methodist Research Institute, 6670 Bertner Avenue, Houston, Texas 77030, USA; [3]Department of Bioengineering, Rice University, 6500 Main Street, Houston, TX 77030, USA; [4]Department of Epigenetics and Molecular Carcinogenesis, Center for Cancer Epigenetics, The University of Texas MD Anderson Cancer Center, 1515 Holcombe Blvd, Houston, TX 77030, USA; [5]Department of Chemistry, Rice University, Houston, 6500 Main Street, Houston, TX 77030, USA; and [6]Department of Cardiothoracic Surgery, Weill Cornell Medical College, Cornell University, Ithaca, NY, USA

Received 29 May 2023; revised 9 November 2023; accepted 12 December 2023; online publish-ahead-of-print 17 January 2024

Time for primary review: 36 days

See the editorial comment for this article 'An emerging epigenetic path towards cardiomyocyte maturation', by W.T. Tay and Y. Wang, https://doi.org/10.1093/cvr/cvae065.

Aims Human pluripotent stem cell-derived cardiomyocytes (iPSC-CMs) provide a platform to identify and characterize factors that regulate the maturation of CMs. The transition from an immature foetal to an adult CM state entails coordinated regulation of the expression of genes involved in myofibril formation and oxidative phosphorylation (OXPHOS) among others. Lysine demethylase 5 (KDM5) specifically demethylates H3K4me1/2/3 and has emerged as potential regulators of expression of genes involved in cardiac development and mitochondrial function. The purpose of this study is to determine the role of KDM5 in iPSC-CM maturation.

Methods and results KDM5A, B, and C proteins were mainly expressed in the early post-natal stages, and their expressions were progressively downregulated in the post-natal CMs and were absent in adult hearts and CMs. In contrast, KDM5 proteins were persistently expressed in the iPSC-CMs up to 60 days after the induction of myogenic differentiation, consistent with the immaturity of these cells. Inhibition of KDM5 by KDM5-C70 -a pan-KDM5 inhibitor, induced differential expression of 2372 genes, including upregulation of genes involved in fatty acid oxidation (FAO), OXPHOS, and myogenesis in the iPSC-CMs. Likewise, genome-wide profiling of H3K4me3 binding sites by the cleavage under targets and release using nuclease assay showed enriched of the H3K4me3 peaks at the promoter regions of genes encoding FAO, OXPHOS, and sarcomere proteins. Consistent with the chromatin and gene expression data, KDM5 inhibition increased the expression of multiple sarcomere proteins and enhanced myofibrillar organization. Furthermore, inhibition of KDM5 increased H3K4me3 deposits at the promoter region of the *ESRRA* gene and increased its RNA and protein levels. Knockdown of ESRRA in KDM5-C70-treated iPSC-CM suppressed expression of a subset of the KDM5 targets. In conjunction with changes in gene expression, KDM5 inhibition increased oxygen consumption rate and contractility in iPSC-CMs.

Conclusion KDM5 inhibition enhances maturation of iPSC-CMs by epigenetically upregulating the expressions of OXPHOS, FAO, and sarcomere genes and enhancing myofibril organization and mitochondrial function.

* Corresponding author. Tel: +713-500-2301; Fax: 713-383-0313, E-mail: priyatansh.gurha@uth.tmc.edu

Graphical Abstract

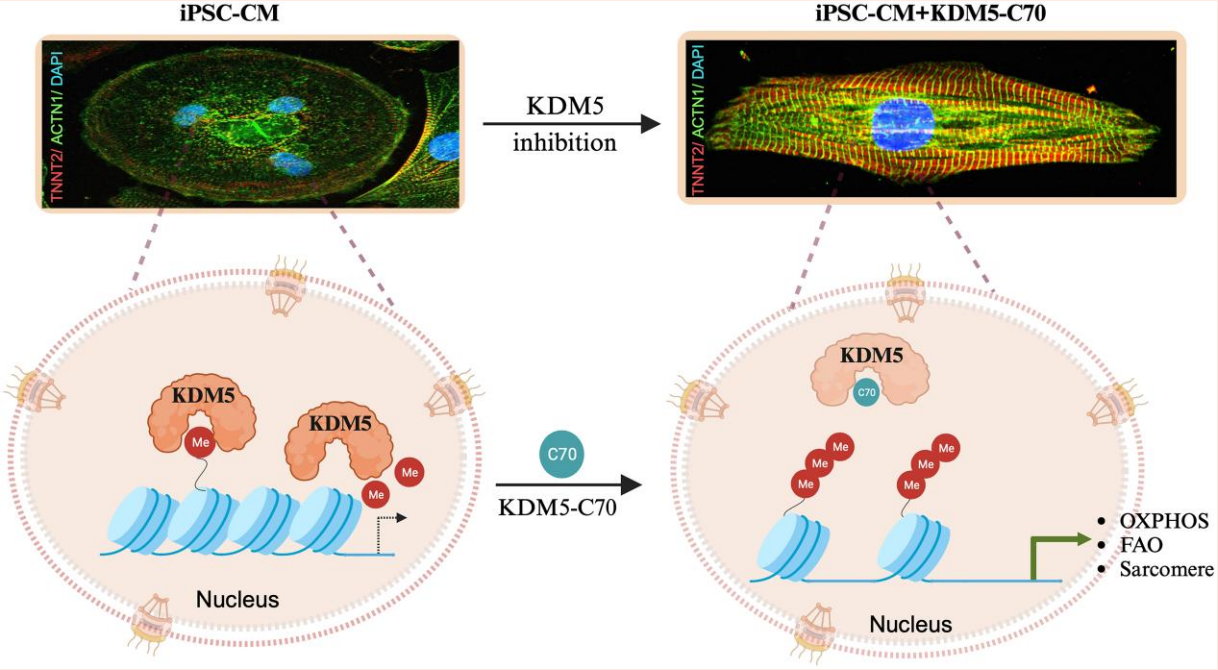

The figure was generated using BioRender.com.

Keywords iPSC-cardiomyocytes • Epigenetics • KDM5 • Histone modification • H3K4me3

1. Introduction

The replicative capacity of human cardiomyocytes (CMs) declines progressively during cardiac development as these cells gradually differentiate towards a mature state. Consequently, the fully differentiated adult CMs possess minimal replicative capacity.[1,2] The loss of replicative capacity of mature CM in the adult heart prevents regeneration and replacement of CMs following myocardial infarction, a leading cause of heart failure.[3–5]

The transition of proliferative and immature CMs to mature and fully differentiated cells involves a series of morphological, metabolic, and functional changes.[6,7] The changes are driven by a switch from a foetal to an adult gene expression profile encompassing genes involved in the myofibrillar organization, mitochondrial oxidative phosphorylation (OXPHOS), fatty acid oxidation (FAO), and an isoform switch in several sarcomere proteins. These changes are also responsible for a shift in metabolic substrate utilization from glucose and lactate to free fatty acids as an energy source. All of these changes improve OXPHOS, sarcomere alignment, and increased contractility, among others.[8]

The recent discoveries that allow efficient differentiation of human pluripotent stem cells (PSCs) into the CM lineage upon induction of the cardiogenic programme have increased interest in the utility of these cells to replace the damaged CMs. However, the immaturity of the induced PSC-derived CMs remains a major bottleneck in their functional utility and has therefore shifted interest to interventions that can enhance iPSC-CM maturation.[9–12]

Current approaches to induce maturation of iPSC-CMs include engineered micropatterned platforms, synthetic cardiac tissue, electrical stimulation, prolonged culture time, and biochemical modification (transcription factor and signalling component alteration), which have exhibited varying degrees of effectiveness.[11] Recent studies have linked chromatin organization and epigenetic modifications such as DNA methylation and histone marks, including the trimethylation of histone H3 at lysine residue 4 (H3K4me3) to CM development and differentiation.[6,7,13–15] In the heart, activating histone modifications, such as H3K4me3, and H3K27ac are enriched in gene promoters associated with CM maturation.[14] H3K4me3 is the main target of histone lysine demethylase 5 (KDM5), which we recently found to be activated in CMs in a mouse model of lamin-associated cardiomyopathy.[16] Members of the KDM5 family, comprised of KDM5A (Chromosome 12), KDM5B (Chromosome 1), KDM5C (X chromosome), and KDM5D (Y-chromosome) are a subfamily of JmjC KDMs, which act as transcriptional corepressors by catalysing the removal of methyl marks from mono-di- an trimethylated H3K4.[17] Recent studies in *Drosophila*, *Caenorhabditis Elegans*, and myoblast cell lines have implicated KDM5 and its homologues, as a regulator of expression of genes involved in organ development and OXPHOS.[18,19] Likewise, we have implicated KDM5 proteins in the suppression of expression of genes involved in OXPHOS and cell cycle progression in the heart.[13,16] In the present study, we tested the hypothesis that KDM5 family members regulate maturation of iPSC-CMs by targeting expression of genes involved in OXPHOS and myofilament formation among others.

2. Methods

Detailed material and methods are provided as Supplementary material online.

2.1 Mice regulatory approvals

The research studies involving mice were conducted in accordance with the National Institutes of Health's guidelines for the care and use of laboratory animals, and they were approved by the Institutional Animal Care and Use Committee (AWC-210013).

2.2 Anaesthesia and euthanasia procedures

Mice were administered anaesthesia Isoflurane from nose cones at a concentration of 3%. The euthanasia of the mice was carried out by subjecting them to 100% CO_2 inhalation followed by cervical dislocation.

2.3 Maintenance and differentiation of human iPSCs

Commercially available human iPSC lines derived from a female donor (Gibco Episomal hiPSC, Gibco, catalog # A18945) and a male donor (ChiPSC22, Cellartis catalog # Y00320, Takara) were maintained in mTeSR1 medium (STEMCELL Technologies, catalog # 85850) in a six-well dish coated with 300 µg/mL Matrigel (Corning, catalog #354230). Cells were checked for mycoplasma contamination using the Mycoplasma detection kit (Southern Biotech, catalog #13100-01) according to the manufacturer's protocol. Cells were split (1:9) when they reached 70–80% confluency using EZ-LiFT Stem Cell Passage Reagent and maintained for 24 h in mTESR1 medium plus 10 µM rock inhibitor Y-27632 (STEMCELL Technologies, cat. 72308). Cells were grown in mTESR1, and the media was changed every 24 h until cells were 75–85% confluent. Experiments were performed in Gibco Episomal hiPSCs (henceforth hiPSC), unless otherwise specified. To initiate differentiation, the iPSCs were treated (Day 0) with 9 µM CHIR (in RPMI/B27 without insulin (RPMI/B27−) for 48 h. Exactly 48 h later (Day 2), the medium was switched to IWP2 (7.5 µM) in RPMI/B27− and on Day 4 to RPMI/B27− only. Then, the medium was changed to RPMI/B27 with insulin (RPMI/B27+) and replaced every 48 h with a fresh media.[20–23] Post-differentiation (Day 9) wells that showed consistent beating throughout were used for subsequent experiments.

2.4 Inhibition of KDM5

After differentiation, iPSC-CMs were lifted from the plate with TrypLE Express (Gibco catalog #12605028), filtered through a 100 µM filter, and placed in RPMI/B27+ medium with a ROCK inhibitor (10 µM) and 10% knockout serum for 24 h. Twenty-four hours later, cells were treated with a series of concentrations of pan-KDM5 inhibitor KDM5-C70[24–26] (Xcessbio catalog # M60192) and 100 µM BSA-conjugated palmitate (1:3), and the medium was changed every 3 days for the next 15 days (D15–D30). The experimental groups to determine KDM5 inhibition efficiency were as follows: (i) iPSC-CMs, (ii) iPSC-CMs plus dimethyl sulfoxide (DMSO) (0.01%), (iii) iPSC-CMs+ KDM5-C70 (0.1 µM), (iv) iPSC-CMs+ KDM5-C70 (0.5 µM), (v) iPSC-CMs+ KDM5-C70 (2 µM), and iPSC-CMs+ KDM5-C70 (10 µM). Optimal KDM5 inhibition, as indicated by H3K4me3 accumulation, was determined, and the subsequent experiments were performed using the optimal concentration of KDM5-C70.

2.5 Structural integrity and sarcomere organization

Cells after treatment for 15 days with KDM5-C70 were removed by using a 1:1 mixture of TrpLE and Accutase (Invitrogen, catalog # A11105-01) and plated on glass coverslips coated with Matrigel (300 µg/mL). Cells were allowed to recover for two days and fixed and stained with anti-ACTN2 and TNNT2 antibodies. Quantitative assessments of circularity, cell area, and perimeter were done by selecting the cell boundaries and using ImageJ software.

2.6 Quantitative real-time polymerase chain reaction

Transcript levels of selected genes were quantitated by qPCR, using gene-specific primer and SYBR Green master mix, and data were normalized to GAPDH or Vinculin (VCL). The sequences of qPCR primers are included in Supplementary material online, *Table S2*.

2.7 RNA sequencing

RNA-seq was performed as published previously.[13,16,27–29] Briefly, the RNeasy Mini Kit was used to isolate total RNA. The samples with an RNA integrity number >9.0 were used for sequencing. The ribosomal RNA was removed, and the RNA was then processed for strand-specific sequencing. Samples were sequenced on an Illumina Nextseq500 using 75 bp paired-end sequencing. STAR aligner was used to map the reads to the human Hg19 genome and Feature Counts programme was used to quantify the reads.[30,31] Genes with a read count of at least one read per million in at least three samples were used for further analysis. The R/Bioconductor package limma-voom[32] was used to calculate the fold change and adjusted *P*-value (*q*-value). Genes showing 1.5-fold change in their transcript levels and a $q < 0.01$ between cells treated with DMSO and KDM5-C70 were considered as differentially expressed genes (DEGs).

2.8 Cleavage under targets and release using nuclease assay

The cleavage under targets and release using nuclease (CUT&RUN) assay was performed at a Core laboratory according to published protocols.[33,34] Briefly, ∼500 000 untreated and KDM5-C70-treated iPSC-CMs were harvested, washed, and attached to activated Concanavalin A-coated magnetic beads, then permeabilized with wash buffer containing 0.05% digitonin. Then cells were incubated with an H3K4me3 antibody, the protein-DNA complex was precipitated, and the DNA was released, purified, and used to generate libraries using NEB Ultra II Library prep kit following manufacturer's instructions. Size distribution of the libraries was determined using the Agilent 4200 TapeStation, and libraries were multiplexed to achieve uniform representation. Libraries were sequenced using the Illumina Nextseq 500 instrument to obtain 15–20 million reads per sample. Processing of the sequencing data was performed using Pluto Bioscience software (https://pluto.bio/), which used Bowtie2 for mapping to the human genome build Hg38 and Sparse Enrichment Analysis for CUT&RUN (SEACR) for peak calling.[35] Consensus peaks from all samples were determined with minimum overlap set of 2 and differential expression of peak counts was performed using Diffbind (summit size 500 bp) on local galaxy instance. Further processing of the data was done on the local galaxy instance that entails mapping the differentially expressed to the corresponding genes using Homer software (annotate peak) and data visualization using the Deep Tools package to identify genome enrichment and functional annotations. The genomic distribution of the differential peaks was also performed by PAVIS (https://manticore.niehs.nih.gov/pavis2/).

2.9 Pathway analysis

Gene set enrichment analysis (GSEA) was performed on normalized counts using the gene sets curated from the Molecular Signature Database (MSigDB) 3.0. Significance was assessed by analysing signal-to-noise ratio and upon 1000 permutations. The data were ordered based on the enrichment score for the gene set with a q-value < 0.05. GSEA for transcription factor binding sites (TFBS) was performed using MSigDB database. Similarly, GSEA was conducted for estrogen related receptor alpha (ESRRA) targets using a gene set specifically created from the publicly accessible ESRRA upregulated targets list derived from cardiac samples.[36] Upstream regulator analysis module of Ingenuity Pathway Analysis software (IPA, QIAGEN Redwood City) was used to identify likely transcriptional regulators based on the DEGs.

2.10 Mito stress assay

After 15 days of treatment (with either DMSO or KDM5 inhibitor), cells were removed upon treatment with a 1:1 mixture of Accutase and TrypLE. At least 40 000 cells/well were plated in Matrigel-coated 96-well dishes in RPMI/B27+ medium containing 100 µM Palmitate, 10% knockout serum, and 10 µM of Y-27632 (ROCKi). After 24 h of incubation, the above medium but without ROCKi was added. Mito stress assays were performed using an Agilent Seahorse machine according to the

manufacturer's protocol. Briefly, 1 h before the assay, cells were washed twice with Agilent Seahorse XF RPMI Basal Medium supplemented with 1 mM sodium pyruvate, 2 mM glutamine, and 10 mM glucose (Agilent Technologies catalog# 103577-100) and incubated in the same medium for 1 h at 37°C in a non-CO_2 incubator. Ports A, B, and C of the XF96 sensor cartridge (Agilent Technologies, catalog 102601-100) were loaded with oligomycin (1.5 μM), carbonyl cyanide-p-trifluoromethoxyphenylhydrazone (2 μM), rotenone, and antimycin A (0.5 μM), respectively. The oxygen consumption rate (OCR) was normalized to the protein concentration determined by the BCA assay. Seahorse Analytics was used to calculate Basal respiration, Spare respiratory Capacity, and Maximal respiration.

2.11 Statistical analysis

The Shapiro–Wilk test was used to determine the normality of the data distribution. Ordinary one-way analysis of variance (ANOVA) was used to analyse normally distributed data, followed by Tukey's multiple pairwise comparison test. The Kruskal–Wallis test was used to analyse data that deviated from the normal distribution, followed by Dunn's pairwise comparisons. GraphPad Prism 9 was used to perform statistical testing. All experiments with the iPSC cells were performed as two–three batches with each batch having three–four replicates of samples obtained from independently treated wells. A subset of gene expression changes was validated by qPCR in an independent cell line ChiPSC22 (see Supplementary material online, *Figures S4G* and *S6A*). RNA-seq and CUT&RUN genomic data are available from the GEO (GSE250210).

3. Results

3.1 KDM5 family of proteins are downregulated upon maturation of murine CMs

Immunoblotting of myocardial protein extracts from 5-day (P5)-, 3-month (P90)-, and 12-month (P180)-old mice showed a progressive decline in the expression levels of KDM5A, KDM5B, and KDM5C in the post-natal period, as these proteins were expressed in the 5-day old but were absent in 3- and 12-month-old mouse hearts (*Figure 1A* and *B*). To determine whether the decline in the heart reflected changes in the expression of these proteins in CMs, immunoblot (IB) was performed on CM protein extracts isolated from P2, P14, P28, and P56 old mice hearts. The KDM5 proteins were expressed in P2 and P14 CMs but their levels were markedly reduced in P28 and P56 CMs (*Figure 1C* and *D*). Thus, the data suggest that KDM5 expression levels decline with the maturation of murine CMs.

3.2 The KDM5 family of proteins are persistently expressed in iPSC-CMs

Given that iPSC-CMs are immature cells and because KDM5 proteins are expressed in the early but not late post-natal CMs, we postulated that KDM5 proteins are involved in maintaining the cells in an immature state. To test this hypothesis, human iPSC-CMs were generated upon differentiation of iPSCs using a chemically defined monolayer protocol through a sequential Wnt activation and suppression protocol.[21,22] The efficacy of the differentiation protocol was determined by analysing expression levels of the molecular markers of iPSC and CMs. As shown previously,[8,10,11] a stage-specific gene expression pattern was observed, which was notable for the induction of the mesodermal lineage marker T-box transcription factor T (aka Brachyury) and MESP1 at D2–D6 (see Supplementary material online, *Figure S1A and B*) and suppression of expression of pluripotency markers *OCT4*, *NANOG*, and *SOX2* (*Figure 1E*). Suppression of expression of the pluripotency markers was associated with increased expression of cardiac transcription factors *NKX2.5*, *GATA4*, and *ISL1* as well as CM markers *ACTC1* and *TNNT2* (*Figure 1E*). The results are consistent with the differentiation stages shown by others.[8,23,37,38]

To determine changes in the expression of the KDM5s at different stages of differentiation, transcript levels of *KDM5A, B, C*, were analysed by qPCR, which showed their expressions at all stages, including the early and late stages of differentiation of iPSC-CMs (*Figure 1E*). *KDM5D* gene which is located on the Y-chromosome was only expressed in male-derived iPSC cell lines and showed a similar expression pattern during iPSC differentiation (see Supplementary material online, *Figure S1C*). To corroborate the findings at the protein level, IB was performed, which showed persistent expression of KDM5A, B, and C proteins at several stages of differentiation of human iPSCs to iPSC-CMs (*Figure 1F* and *G*). Furthermore, immunofluorescence (IF) co-staining of iPSC-CM with anti-KDM5 and anti-TNNT2 antibodies, the latter a marker of CMs, confirmed KDM5 expression in the iPSCs and iPSC-CMs (*Figure 1H*). Moreover, IF staining showed that KDM5s were predominantly located in the nucleus (*Figure 1H*). These findings showing persistent expression of the KDM5 proteins in immature iPSC-CMs.

3.3 Inhibition of KDM5 proteins induces expression of the mature CM gene programmes

To ascertain whether the continued expression of KDM5s contributes to the immaturity of iPSC-CMs, we inhibited KDM5 proteins with a small molecule inhibitor KDM5-C70. Because KDM5s are expressed *in vivo* in immature CM but not in adult CM, immature but committed CM was used in the studies. Gene expression was analysed at different time points of iPSC differentiation, which showed increased expression levels of transcription factors *IRX4, HAND1, NRF2, TBX5,* (see Supplementary material online, *Figure S1C*) and *GATA4* and decreased *ISL1* levels at Day 15 post differentiation (*Figure 1E*). Consistent with these data, in the Day 15 iPSC-CM, the levels of foetal isoforms of myosin (*MYL7*, *MYH6*) and troponin (*TNNI1*) were comparatively higher than the levels of their corresponding adult isoforms (*MYL2*, *MYH7*, *TNNI3*) (see Supplementary material online, *Figure S1D*). These findings are consistent with the pattern observed in immature but committed CMs. IF labelling of cells on Day 15 using antibodies against TNNT2 and ACTN2 showed that 88 ± 9.3% of cells expressed TNNT2 (see Supplementary material online, *Figure S1E and F*). Taken together the D15 iPSC-CM, representing immature CMs, were selected for treatment with a pan-KDM5 inhibitor KDM5-C70, which is a cell-permeable derivative of KDM5-C49 and inhibits the activity of all KDM5 proteins by competing with α-ketoglutarate for binding to the active site.[24,25] To obtain the effective dose for inhibition, iPSC-CMs were treated with four different concentrations of the KDM5-C70 (10, 2, 0.5, and 0.1 μM) for 2 weeks. The treatment duration was chosen to inhibit KDM5s when their expression levels were the highest (days 15–30). Cells treated with vehicle (0.01% DMSO) and untreated cells were included as controls. Inhibition of KDM5, as expected, led to a dose-dependent increase in the H3K4me3 levels, as determined by IB (*Figure 2A*). The highest dose of KDM5-C70 increased the steady-state level of H3K4me3 by 11.93 ± 1.6-fold (*Figure 2A* and *B*). The minimum dose that achieved a maximum effect was determined to be 0.5 μM, which caused a 9.9 ± 1.6-fold increase in H3K4me3 levels compared with DMSO-treated cells. No discernible changes in the levels of other histone methylations such as H3K27me3 and H3K9me3 were observed after 7 days of treatment of iPSC-CMs with 0.5 μM of KDM5-C70 (see Supplementary material online, *Figures S2A and B*). Finally, IF staining showed nuclear accumulation of H3K4me3 in the treated group (0.5 μM KDM5-C70 group) compared with the DMSO or non-treated group (*Figure 2C*). Because KDM5-C70 at a dose of 0.5 μM was sufficient to suppress KDM5 activity without causing non-specific effects, this dose was chosen for the subsequent experiments.

To identify genes whose expressions were regulated by the KDM5 family of proteins, iPSC-CMs were treated with KDM5-C70 (0.5 μM) for 2 weeks and analysed for gene expression changes by RNA-Seq. The untreated and DMSO-treated cells served as controls. Multidimensional scaling (MDS) plots of the RNA-seq dataset showed a clear separation of the treated and control groups, whereas the two control groups were not distinct from each other (*Figure 2D*). Likewise, there were no DEGs, defined

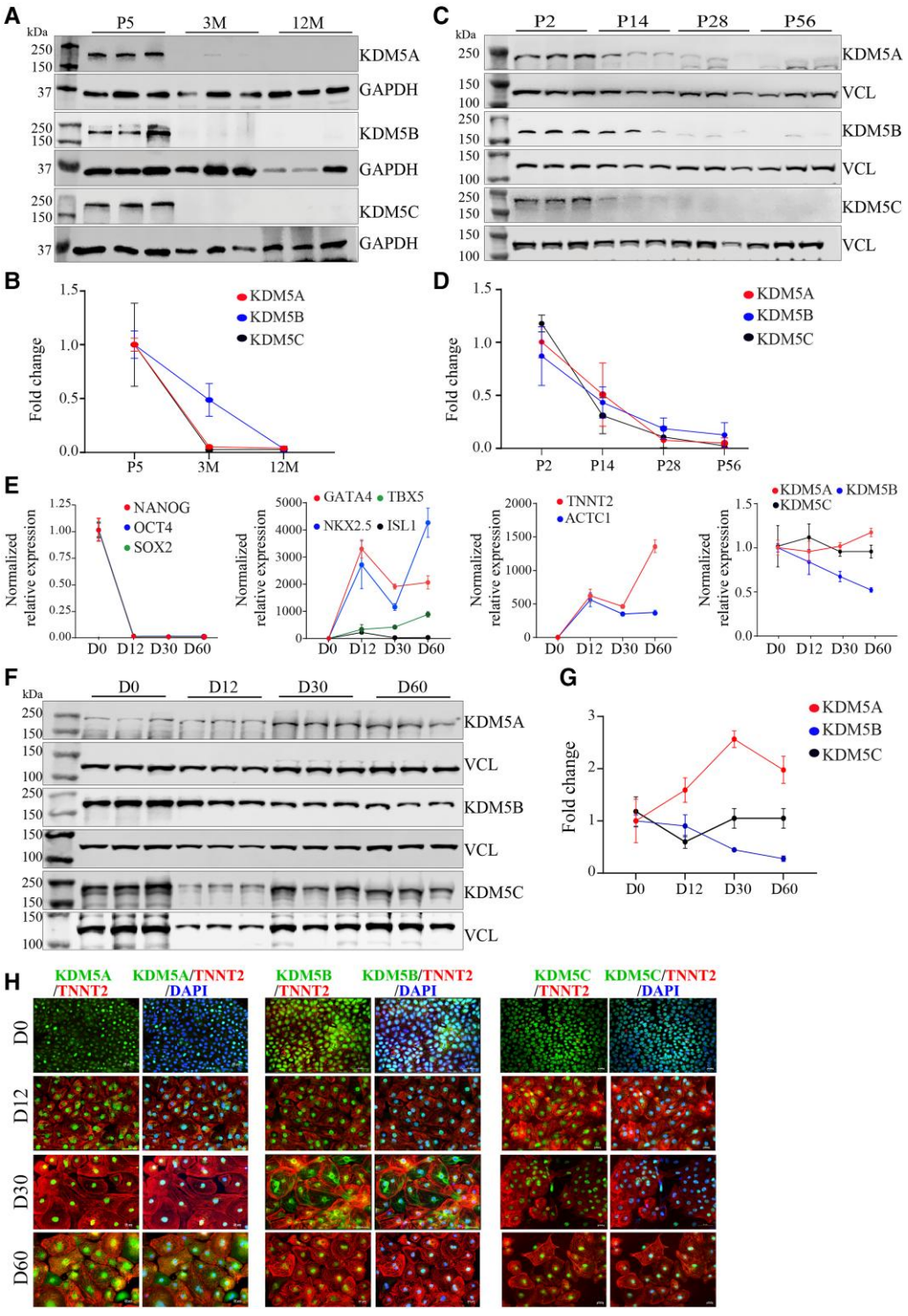

Figure 1 Expression of KDM5A, B, and C in immature and mature CMs. (*A*) Immunoblot (IB) analysis from whole heart extracts showing the expression of KDM5A, KDM5B, and KDM5C in the neonate (P5) and their absence in heart samples from adult mice. GAPDH was used as a loading control. (*B*) Respective quantitative data for KDM5A, B, and C normalized to GAPDH levels from whole heart extracts. (*C*) IB analysis of KDM5A, B, and C levels in mouse CMs isolated from newborn (P2), 2-week (P14), 4-week (P28), and 8-week (P56) mouse hearts. (*D*) Corresponding quantitative data for KDM5A, B, and C from cardiac myocytes normalized to VCL. (*E*) qPCR analysis of RNA extracted at different time points of differentiation of human iPSCs towards cardiac lineage. The relative expression levels of pluripotent markers, cardiac transcription factors, and CM lineage markers at different stages of differentiation are shown. The expression levels of *KDM5A*, *5B* and *5C* at the indicated time points are also shown. (*F*) IB analysis of KDM5A, 5B, and 5C levels from extracts obtained at different time points of iPSC differentiation to CM. (*G*) Quantitative data showing consistent expression of KDM5A, B, and C proteins in iPSC and at all stages of iPSC differentiation towards CM normalized to VCL. (*H*) IF staining of cells with anti-KDM5A, B, or C (green) and anti-TNNT2 antibodies (red) and DAPI (blue) showing the expression and nuclear localization of KDM5 proteins at all stages of differentiation.

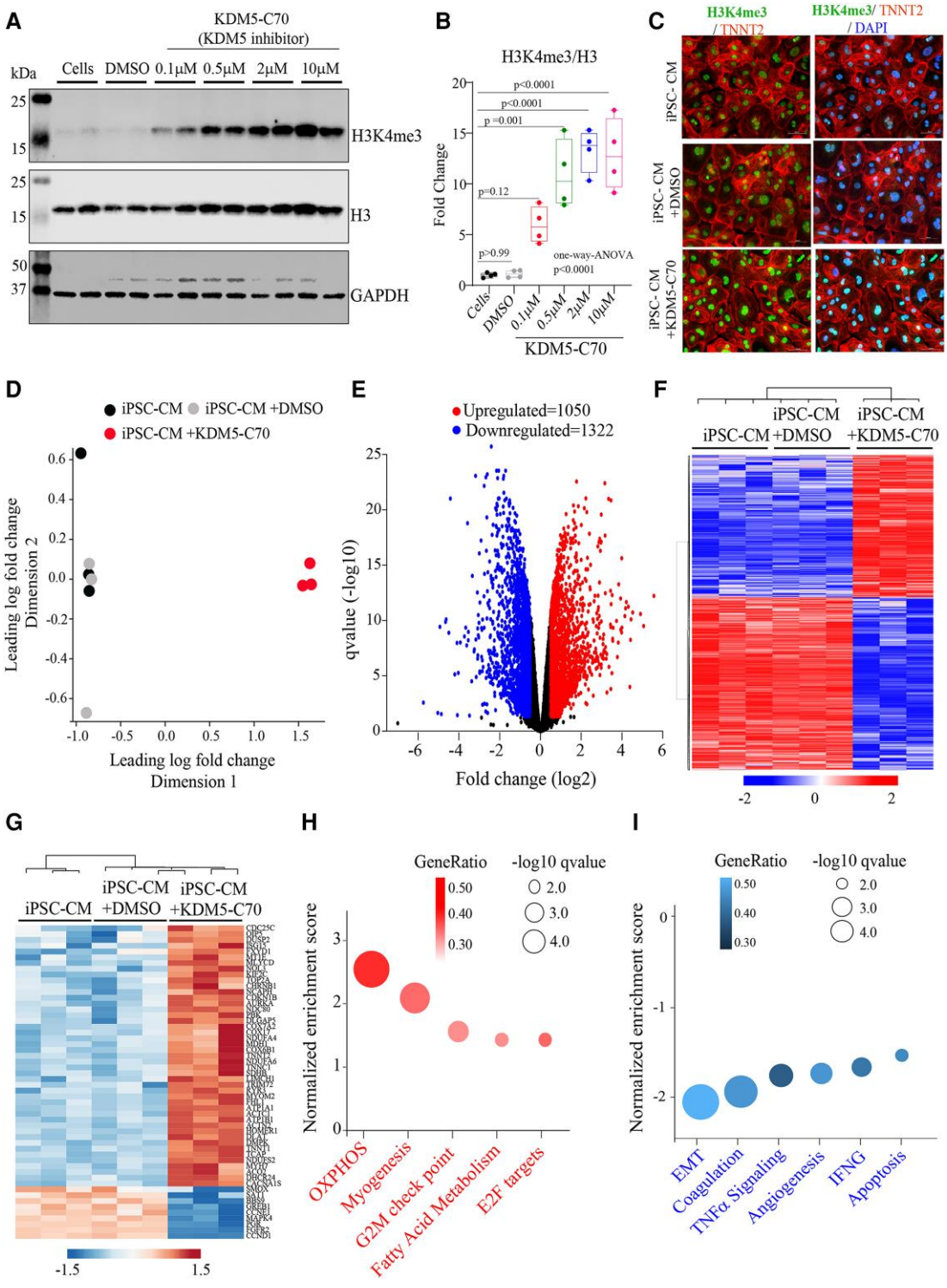

Figure 2 Effect of KDM5 inhibition on iPSC-CM gene expression. (*A*) Immunoblot showing H3K4me3 levels after treatment of iPSC-CMs with different concentrations of the KDM5 inhibitor (KDM5-C70). Cells treated with vehicle (0.01% DMSO) and untreated cells served as controls. (*B*) Changes in the level of H3K4me3 relative to H3 for the data shown in *A*. (*C*) IF staining using anti-H3K4me3 (green) and anti-TNNT2 (red) antibodies and DAPI (blue) (*D*) MDS plot of RNA-seq data showing the separation of iPSC-CMs and DMSO from the KDM5-C70-treated samples. (*E*) Volcano plots obtained from RNA-seq data showing DEGs and the significance level in KDM5-C70 compared with untreated control iPSC-CMs. The differentially upregulated genes are shown in red, while those that are downregulated are shown in blue and those that remain unchanged are shown in black. (*F*) Heatmap and hierarchical clustering of DEGs in the indicated groups. (*G*) Heat plot showing the expression pattern and differential expression status of KDM5A, and B predicted targets after KDM5-C70 treatment. (*H* and *I*) GSEA after KDM5-C70 treatment showing the activated (*H*) or inhibited (*I*) hallmark gene signature. The *Y*-axis in the graphs represents the Normalized Enrichment Score, the colour intensity represents the number of genes involved, and the size indicates the level of significance for each pathway.

at a $q < 0.01$ and 1.5-fold change, between the two control groups (untreated vs. DMSO). In contrast, inhibition of KDM5 was associated with the differential expression of 2415 genes when compared with untreated control cells and 2427 genes compared with the DMSO-treated cells. A total of 2372 genes were differentially expressed in the KDM5-C70 iPSC-CMs when compared with both DMSO and untreated cells (1050 upregulated and 1322 downregulated) (*Figure 2E*). Heat plots for the genes that were differentially expressed in the KDM5-C70-treated when compared with both DMSO and untreated cells are depicted in *Figure 2F*. The DEGs were analysed for the expression of known KDM5A and KDM5B target genes, which showed increased expression levels in the iPSC-CMs treated with KDM5-C70, in agreement with the known inhibitory role of the KDM5 proteins on gene expression (*Figure 2G*). GSEA of the DEGs predicted the upregulation of genes encoding OXPHOS, fatty acid metabolism, and sarcomere proteins (*Figure 2H*). The downregulated genes predicted suppression of the expression of genes involved in extracellular matrix (ECM) formation and inflammation (*Figure 2I*).

3.4 Identification of H3K4me3 enriched genomic sites in iPSC-CMs

Since KDM5s are histone demethylases that specifically target H3K4me1/2/3, genomic loci that are enriched with the H3K4me3 serve as a surrogate for the KDM5 binding sites. To identify the genome-wide H3K4me3 enriched sites, iPSC-CMs treated with the KDM5-C70 and untreated control cells were analysed by CUT&RUN assay. Approximately, 15 million reads per sample were obtained, which were uniquely mapped to the human genome (GRCH38). Peaks were accessed using the SEACR programme, which resulted in the identification of a total of 13 573 consensus peaks. Heat maps depicting the signal distribution of the H3K4me3 peaks over IgG in the control and KDM5-C70-treated cells are depicted in *Figure 3A*, which showed a significant signal enrichment in the H3K4me3 antibody group when compared with the background signal in the IgG groups. The heat map of the individual samples is shown in Supplementary material online, *Figure S3A and B*. Differential enrichment analysis ($q < 0.05$) identified 4373 upregulated and 334 downregulated peaks in iPSC-CMs treated with the KDM5 inhibitor compared with the control group (*Figure 3B*).

The genomic distribution of the H3K4me3 peaks showed marked enrichment at the promoter and transcription start site (TSS) upstream regions with a subset of peaks enriched at the intronic cis elements (*Figure 3C*). In addition to the enrichment of H3K4me3 peaks in the promoter and upstream regions, there was a broader signal distribution of H3K4me3 across the TSS in the KDM5 inhibition group (*Figure 3A* and *D*). These results imply that inhibition of KDM5 alters the genome-wide distribution of H3K4me3, increased peak intensity (size), and peak width in iPSC-CMs.

To gain insight into the biological significance of these findings, differentially enriched H3K4me3 peaks were analysed for their effect on gene expression after KDM5 inhibition. Integration of the RNA-seq and the CUT&RUN dataset was performed by analysing the upregulated and downregulated peaks against the DEG. This unbiased analysis showed that of 1126 DEGs, 457 had increased H3K4me3 deposits at their promoter and upstream regions after KDM5 inhibition (*Figure 3E*). The downregulated genes upon treatment with the KDM5 inhibitor did not show reduced deposition of H3K4me3 at their promoter and upstream regions. The data suggest that inhibition of KDM5 led to dysregulation of gene expression in an H3K4me3-dependent manner.

3.5 Inhibition of KDM5 induces expression of genes encoding sarcomere and myofibrillar organization in the hiPSC-CMs

Analysis of the RNA-seq data showed upregulation of expression of genes involved in myogenesis in the iPSC-CMs treated with KDM5-C70 compared with controls. Similarly, GO analysis showed that genes involved in sarcomere and myofibrillar organization were highly enriched in the iPSC-CMs treated with KDM5-C70 (*Figure 4A*). Furthermore, independent analysis of the transcript levels of several sarcomere genes by qPCR confirmed induction of maturation-specific sarcomere genes *TNNI3* (approximately five-fold), *MYL2* (approximately threefold), *MYH7* (~1.4-fold), *TNNT2* (~1.4-fold), *MYOZ2* (approximately two-fold), *TPM1* (~1.6-fold) and *ACTC1* (~1.6-fold) as shown in Supplementary material online, *Figure S4A*. Likewise, the gene expression ratio of adult/foetal myosin heavy chain, myosin light chains, and troponin I isoforms were higher in KDM5 inhibition groups when compared with controls or DMSO group (see Supplementary material online, *Figure S4B*). To determine whether changes in gene expression correspond to changes in H3K4me3 levels, selected differentially expressed sarcomere genes were analysed for the H3K4me3 accumulation at their promoters. Overall, 27 sarcomeric/myogenesis genes showed a concordant increase in their transcript levels and H3K4me3 peaks at their promoters in iPSC-CMs treated with KDM-C70. The corresponding heat map is shown in *Figure 4B*. Selected examples of H3K4me3 accumulation at the promoter regions of the sarcomere genes implicated in CM maturation namely, *MYH7*, *MYL2*, *TNNI3*, and *MYOM2* are shown in *Figure 4C*.[6,7,39] The data suggest that KDM5 regulates expression genes involved in sarcomere formation, through genome-wide regulation of H3K4me3 at the target locus in the iPSC-CMs.

Protein levels of selected sarcomere genes were determined by IB, which showed increased expression of MYL2 (4.2 ± 1.1-fold), TNNI3 (4.2 ± 0.4-fold), MYH7 (2.46 ± 0.1-fold), and MYOM2 (1.8 ± 0.3-fold) after KDM5-C70 treatment (*Figure 4D* and *E*). To quantitatively assess differences in cell morphology of iPSC-CMs upon treatment, cell surface area, cell perimeter, and circularity index were measured. Cells treated with KDM5-C70 showed significantly less circularity, indicating that KDM5-C70 caused the elongation of these cells (*Figure 4F* and *G* and Supplementary material online, *Figure S4C*). Cells treated with KDM5-C70 were ~30% smaller than the untreated or DMSO-treated cells. A hallmark of CM maturation is the assembly of organized arrays of myofibrils. To visualize the regularity of myofibrillar assembly, iPSC-CMs were immunostained for the sarcomere protein actinin (ACTN2) and troponin T2 (TNNT2). Treatment with KDM5-C70 resulted in regularly arranged sarcomeres, while control iPSC-CMs showed sparse disorganized sarcomeres (*Figure 4F* and Supplementary material online, *Figure S4C*). Finally, upon suppression of KDM5, there was an upward trend in the percentage of cells exhibiting binucleated myocytes in the treated group when compared with the control groups (see Supplementary material online, *Figure S4D*). Since the ECM plays an important role in iPSC-CM maturation, we plated the iPSC-CMs on another ECM prepared by PDMS/Matrigel coating of glass coverslips.[40,41] The results were remarkable for an increased number of elongated cells with organized sarcomeres in the KDM5-C70-treated groups compared with the untreated cells on the same substrate (see Supplementary material online, *Figure S4E and F*). The expression of sarcomere genes in another cell line after KDM5 inhibition showed similar upregulation of sarcomere genes as shown in Supplementary material online, *Figure S4G*.

Transcript levels of genes encoding cardiac ion channels, gap junction protein, and calcium handling genes were induced after KDM5-C70 treatment (see Supplementary material online, *Figure S5A*). IB analysis showed an increased expression of PLN but no significant changes in amounts of ATP2A2 or RYR2 as shown in Supplementary material online, *Figure S5B and C*. IF staining of CX43 showed increased expression and localization of CX43 upon KDM5 inhibition (as shown in Supplementary material online, *Figure S5D*). To determine if KDM5 inhibition had a functional effect on CM excitation-contraction coupling, we simultaneously measured action potential, Ca^{2+} transients, and contractility elicited by electrical field stimulation. The iPSC-CMs (after 15 days of treatment with vehicle or KDM5-C70) were, loaded with FluoVolt and Cal-590AM, and their fluorescence intensity was measured using an IonOptix instrument. A pixel intensity algorithm detecting changes in brightfield contrast was used to assess contractility. Cells were continuously paced at 37°C at a frequency of 1 Hz to achieve steady-state levels. KDM5-C70-treated CMs exhibited a faster action

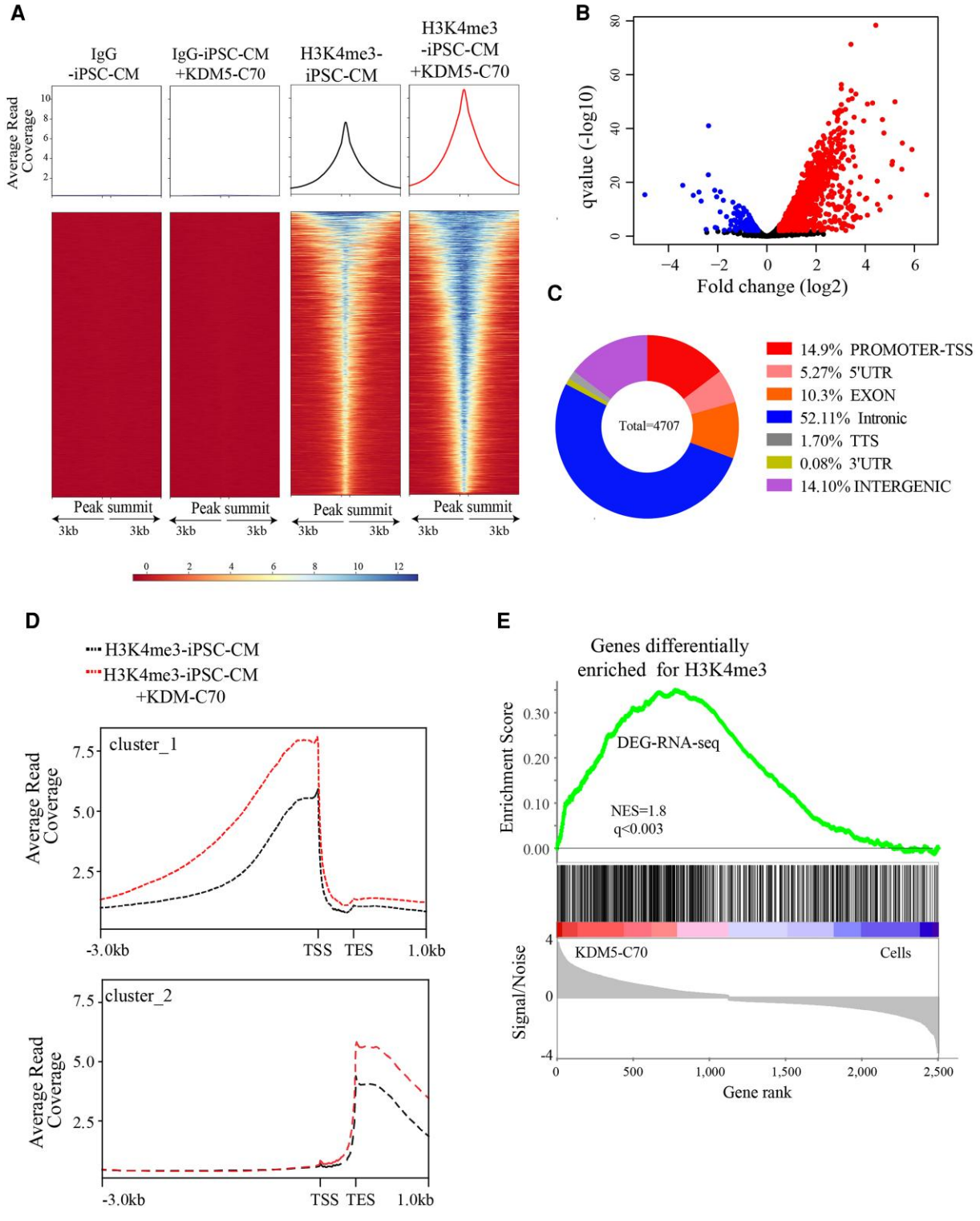

Figure 3 Effect of KDM5 inhibition on genome-wide H3K4me3 distribution. (*A*) Heat plot showing cumulative signal intensity for H3K4me3 and IgG in treated and untreated samples. The upper panels show the average profile of the peaks. The lower panels show read density heatmaps around 3Kb from the peak centres. (*B*) Volcano plot showing differentially H3K4me3 peaks in the KDM5-C70-treated vs. control groups. Peaks that are differentially upregulated (higher signal intensity) are shown in red, while downregulated peaks are shown in blue. (*C*) Genome-wide distribution of differentially enriched H3K4me3 peaks. Promoter and upstream regions are defined as the region 3 kb upstream and 1 kb downstream from the start of transcription. (*D*) Distribution of peaks around the TSS, gene body and downstream to gene body in control cells (black) and KDM-C70-treated cells (red). (*E*) GSEA plots showing the correlation of RNA levels of DEGs with the genes that have differentially higher H3K4me3 deposits in KDM5-C70-treated vs. control groups.

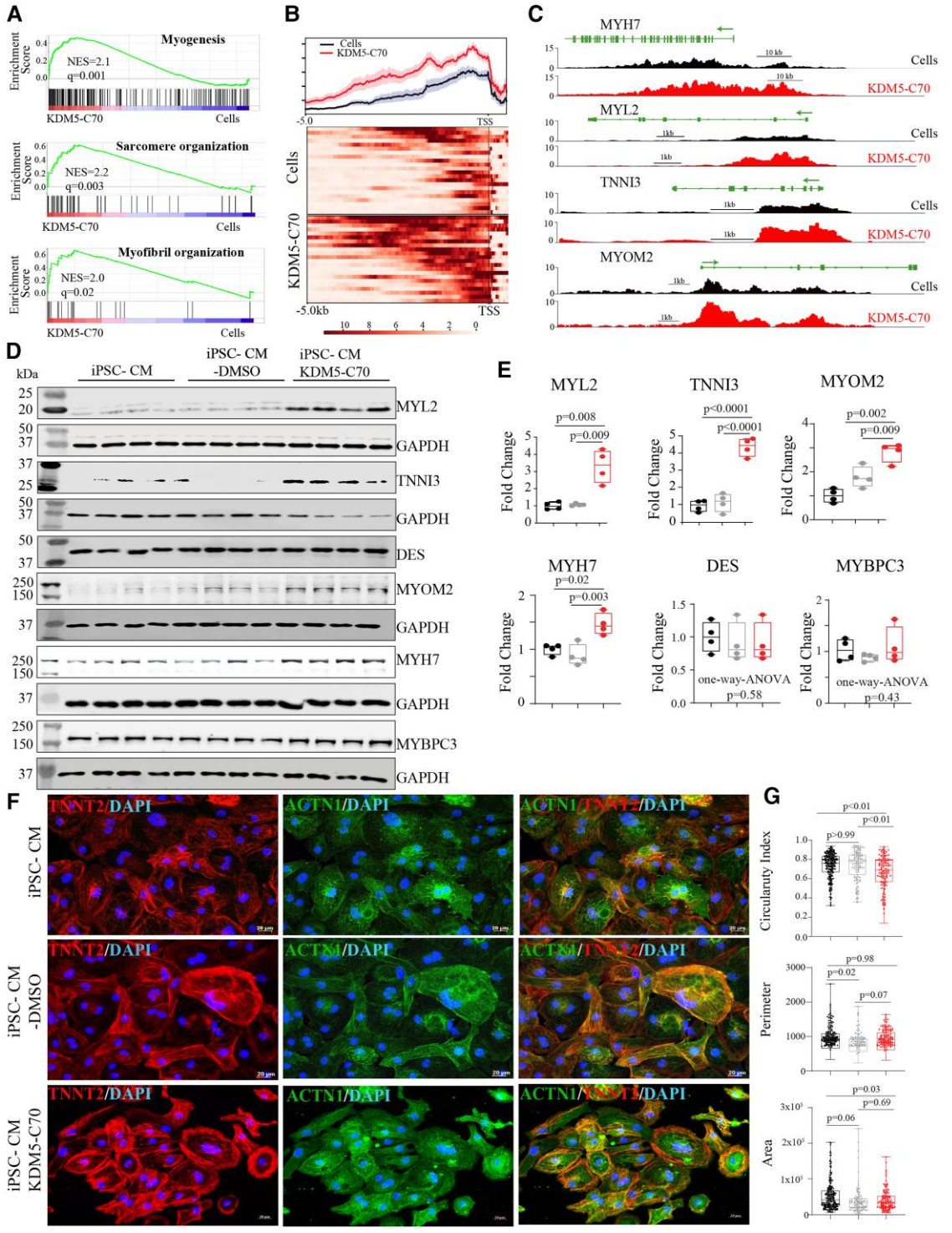

Figure 4 Effect of KDM5 inhibition on sarcomere gene programme. (*A*) GSEA and GO analysis of DEGs showing induction of the gene programme involved in myogenesis, and myofilament formation. (*B*) Distribution of H3K4me3 peak density at the TSS of sarcomere genes differentially expressed in KDM5-C70-treated (red) vs. control (black) samples and heat plot showing the signal intensity of H3K4me3 in the upstream regions of sarcomere genes in control and KDM5-C70-treated samples. (*C*) Integrative genomics viewer (IGV) genome browser trace of H3K4me3 showing peak intensity at the promoter and upstream regions of selected sarcomere genes in control and treated samples. (*D–E*) IB analysis showing increased expression of MYL2, TNNI3, MYOM2, and MYH7 and no changes in Desmin (DES) and MYBPC3 in KDM5-C70-treated groups. (*F*) IF staining with anti-TNNT2 (red), anti-ACTN1 (green), and DAPI (blue) showing sarcomeres and a prominent striated pattern in KDM5C-70-treated cells. Cells were plated on a Matrigel-coated glass coverslip. (*G*) Calculated circularity index (0 = oblong and 1 = circle), area, and perimeter for control, DMSO, and KDM5-C70-treated samples.

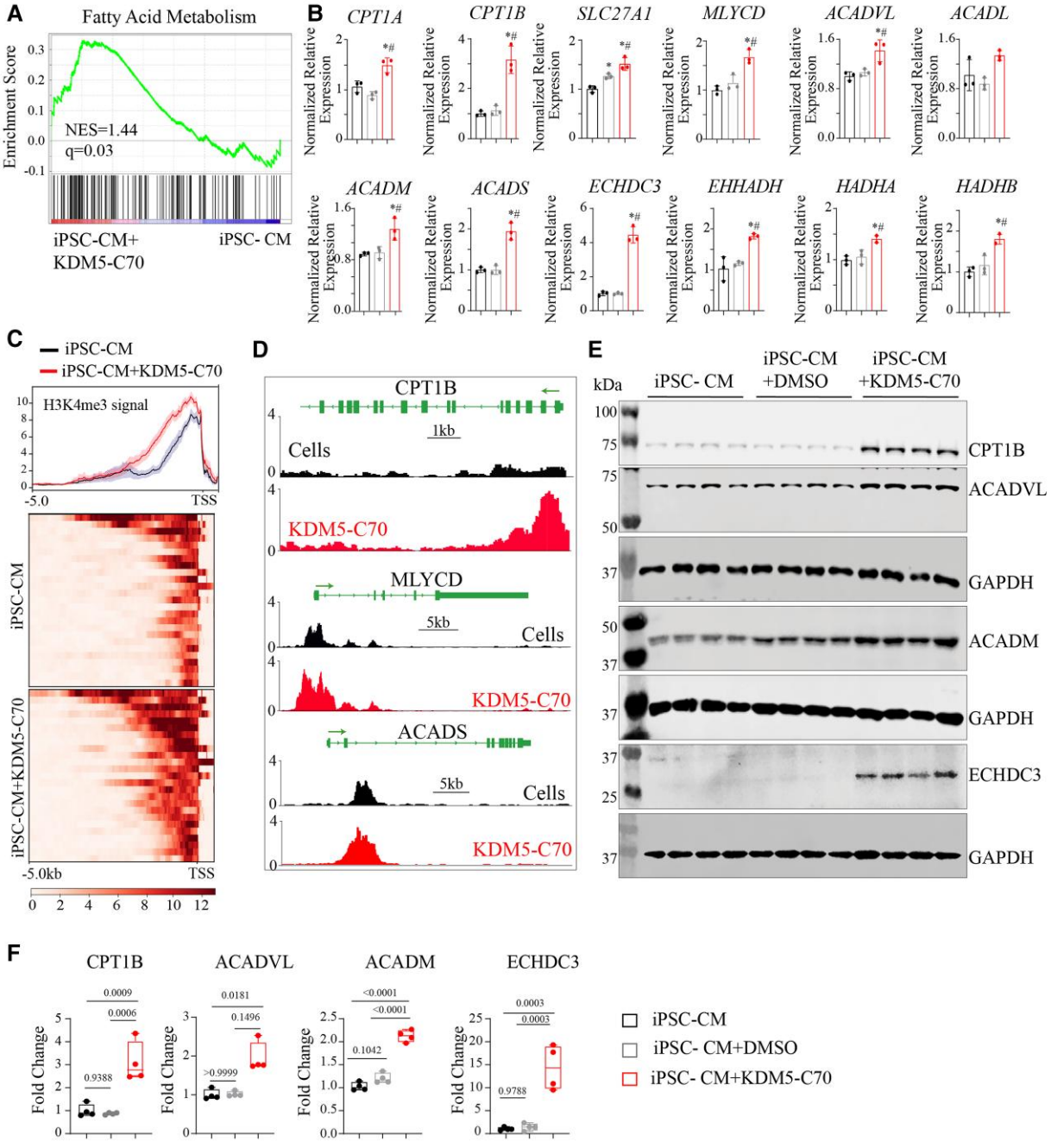

Figure 5 KDM5 inhibition leads to induction of FAO gene programme. (*A*) GSEA showing activation of fatty acid metabolism gene signature. (*B*) qPCRs of genes involved in fatty acid transport and oxidation demonstrate induction in KDM5-C70-treated cells. (*C*) Heat plots showing distribution profile of peak density and peak width enrichment near the TSS of fatty acid metabolism genes in cells and KDM5-C70-treated samples. (*D*) IGV genome browser traces of H3K4me3 on selected genes involved in fatty acid metabolism in the control (black) and KDM5-C70-treated samples (red). (*E*) IB analysis showing increased expression of the fatty acid transporter CPT1B, and the enzymes involved in beta-oxidation of fatty acids namely ACADVL (Kruskal–Wallis test $P = 0.0048$), ACADM and ECHDC3 in treated cells. (*F*) Quantitative data showing the fold change in the expression of proteins as shown in *E*. Pairwise corrected *P*-values are shown in the figure.

potential upstroke velocity, longer action potential duration, increased Ca^{2+} transients, reflected in an increased area under the curve, and increased contractility with faster kinetics of contraction and relaxation compared with those observed treated with a vehicle (see Supplementary material online, *Figure S5E–G*). Together, this evidence suggests that inhibition of KDM5 improves iPSC-CM excitation-contraction coupling.

3.6 Inhibition of KDM5 enhances FAO and OXPHOS and in hiPSC-CMs

Consistent with the metabolic switch during maturation of CMs, KDM5-C70 treatment induced the expression of several genes involved in fatty acid metabolism (*Figure 5A*).[6,7,42] RNA-seq analysis showed that

genes involved in different stages of fatty acid metabolism were induced by KDM5-C70 treatment. qPCR analysis for the transcripts of genes involved in fatty acid transport *CPT1A*, *CPT1B*, *SLC27A* showed a 1.5- to 3-fold increase upon KDM5 inhibition. Likewise, genes involved in acyl-CoA degradation via oxidation, such as *ACADVL*, *HADHA*, and *HADHB*, were induced by KDM5-C70 treatment (*Figure 5B*). The H3K4me3 signal for these specific genes showed a predominant accumulation at their promoter regions in the cells treated with the KDM5 inhibitor (*Figure 5C*). *Figure 5D* shows a selection of peaks demonstrating both increased size and width at the promoters of the *CPT1B, MLYCD,* and *ACADS* genes. Finally, the protein levels of CPT1B (2.09 ± 0.3), ACADVL (seven-fold), ACADM (2.12 ± 0.1), and ECHDC3 (13.3 ± 2.2) were increased as shown in *Figure 5E* and *F*. Similar changes were also observed in iPSC-CM derived from an independent cell line (see Supplementary material online, *Figure S6A*). Next, to determine whether KDM5 governs CM maturation programme by FAO and sarcomeric gene programme separately or exclusively, FAO was suppressed alongside KDM5 inhibition. The experiment involved the pharmacological inhibition of FAO using etomoxir (ETO). The iPSC-CMs were simultaneously treated with ETO and C70 for 2 weeks. The control groups consisted of untreated cells and or cells treated with KDM5-C70 alone. qPCR analysis showed that following treatment with ETO, there was a decrease in the expression of only a specific set of genes, including MYOM3, CAV3, and Desmin (DES) in the treated group (see Supplementary material online, *Figure S6B*). Nevertheless, the transcript levels of various additional sarcomeric genes and FAO exhibited no significant alterations (see Supplementary material online, *Figure S6B*). The results suggest that KDM5 plays a crucial role in initiating the gene programme associated with the maturation of iPSC-CMs and regulates both FAO genes and sarcomeric genes concurrently.

Transcripts of genes involved in OXPHOS were increased in iPSC-CMs treated with KDM5-C70, as evident from the GSEA plots shown in *Figure 6A* and the qPCR data shown in *Figure 6B* and IB for selected Complex I–V proteins shown in *Figure 6C* and *D*. However, mitochondria content of the cells as determined by, mitochondrial DNA and Mito tracker FACS, was not changed (see Supplementary material online, *Figure S7A–C*). To determine the effect of gene expression changes on OXPHOS, an extracellular flux assay was performed to measure real-time OCR (*Figure 6E*). Inhibition of KDM5 in the iPSC-CMs increased the basal respiratory rate and there was a two-fold difference in maximal respiration (*Figure 6F*). There was also a two-fold increase in spare capacity and also an increase in ATP-linked respiration, between the KDM5-C70-treated and untreated cells (*Figure 6G*), demonstrating improved aerobic respiration and ATP production in the KDM5-C70-treated cells. Taken together, these results support the role of KDM5 in iPSC-CM metabolic maturation through FAO and OXPHOS regulation.

In order to identify the downstream effector of KDM5 inhibition, and given that transcription factors function in conjunction with histone demethylases,[43–47] we analysed the enrichment of TFBS in the DEGs following KDM inhibition. This analysis revealed an enrichment of ESRRA, SRF, and MEF2 motifs in DEG. Among these, it has been demonstrated that ESRRA functions as a regulator of gene expression related to sarcomere organization, FAO, and OXPHOS in CMs.[36,48,49] The RNA sequencing data showed a significant upregulation of *ESRRA* gene expression following the inhibition of KDM5. qPCR analysis indicated a 2.1-fold increase (±0.2) in the expression of *ESRRA* upon KDM5-C70, as depicted in Supplementary material online, *Figure S8A*. In accordance with alterations in the RNA levels, the protein levels of ESRRA were shown to be increased 2.4 ± 0.36 following treatment with KDM5-C70, as depicted in Supplementary material online, *Figure S8B and C*. Similarly, treatment of a second independent iPSC-CM line with KDM5-C70 increased *ESRRA* expression (see Supplementary material online, *Figure S8D*). Likewise, GSEA demonstrated that the treatment with KDM5-C70 led to the induction of transcript levels of ESRRA target genes (see Supplementary material online, *Figure S8E*). The CUT-and-RUN data showed the presence of H3K4me3 enrichment in the promoter region of *ESRRA*, as depicted in Supplementary material online, *Figure S8F*. The summation of the data suggests activation of ESRRA upon KDM5 inhibition. Therefore, to ascertain if a subset of the effects resulting from KDM5 inhibition may be attributed to ESRRA, we employed siRNAs to knock down ESRRA subsequent to treating iPSC-CM with KDM5-C70. ESRRA was effectively downregulated, resulting in ~90% decrease in both untreated control cells and cells treated with KDM5-C70, as shown in Supplementary material online, *Figure S8G*. The suppression of ESRRA resulted in a reduction in the expression of sarcomere genes, such as TNNI3, MYL2, and TCAP, as well as the FAO genes ACADM and ACADVL, when compared with cells treated with C70. However, expression levels of other genes remained unchanged upon ESRRA knockdown (see Supplementary material online, *Figure S8H*). Collectively, our findings indicate that the inhibition of KDM5 results in the stimulation of the gene programme associated with the maturation iPSC-CMs a subset of which through the activation of ESRRA, which in turn may further enhance the expression of genes related to maturation.

4. Discussion

The results demonstrate that inhibition of KDM5 activity by a pan-KDM5 small molecule inhibitor KDM5-C70 is sufficient to induce H3K4 methylation, increase H3K4me3 level, and activate gene expression. Inhibition of KDM5 in immature iPSC-derived CMs resulted in a gene expression reprogramming that resembles that of mature CM. Specifically, inhibition of KDM5 led to the induction of genes involved in FAO and OXPHOS, leading to improved FAO and OCR in iPSC-CMs. Similarly, genes encoding sarcomere proteins were induced by KDM5 inhibition, resulting in the striated organization of the sarcomere. Mechanistically, the data suggest that KDM5 inhibition shifted the iPSC-CM towards maturation (i) through direct regulation of genes involved in FAO, OXPHOS, and sarcomere formation and (ii) additionally by regulation of the transcription factors like ESRRA, a known regulator of CMs maturation.[36,50] Our results are consistent with recent reports showing the role of ESRRA in CM maturation mainly through the regulation of genes involved in sarcomere and FAO and creation of an epigenetic link to the maturation gene programme. It has been proposed that KDM5A both induces and represses mitochondrial biogenesis and function; however, its role in regulating the energy metabolism of CMs is unknown. Recently, we showed that in a mouse model of laminopathies, KDM5A was induced and associated with the repression of its target genes involved in OXPHOS.[16] Data in the present study indicate that the KDM5 family of proteins regulate energy metabolism in CMs through multiple target genes involved in mitochondrial function and fatty acid uptake and oxidation. Finally, the data show that a mutually exclusive control of FAO and sarcomere genes by KDM5s. Specifically, the inhibition of FAO by ETO was found to have only a moderate impact on the expression of sarcomere genes.

Our studies also point to the role of KDM5 in the regulation of the expression of sarcomere proteins. Inhibition of KDM5s resulted in increased deposition of H3K4me3 on the promoter regions of several sarcomere genes, namely *MYL2*, *TNNI3*, and *MYH7*, among others, and led to an increase in their RNA and proteins levels. These expression changes are conserved and vital for the transition from prenatal to postnatal CMs and are therefore an integral part of the maturation process of CMs in adults. These gene expression changes were associated with better sarcomere alignment and contractility. Nevertheless, overall findings are intriguing and will open new avenues for targeting the sarcomere gene expression by modulating KDM5 activities upon further investigation and validation in the *in vivo* models.

The molecular basis of KDM5-mediated gene regulation in CMs remains unknown. Our data indicate that KDM5s are one of the major regulators of H3K4me3 demethylation in iPSC-CMs. Likewise, our data points to a direct role of H3K4me3 in gene regulation as the changes in the H3K4me3 levels after KDM5-C70 treatment strongly correlate with changes in gene expression. The precise role of H3K4me3 in gene expression might be context-dependent, but recent data have shown that H3K4me3 regulates promoter-proximal pausing of RNA polymerase II.[51] Our data indicate that KDM5 inhibition reprogrammes gene expression towards

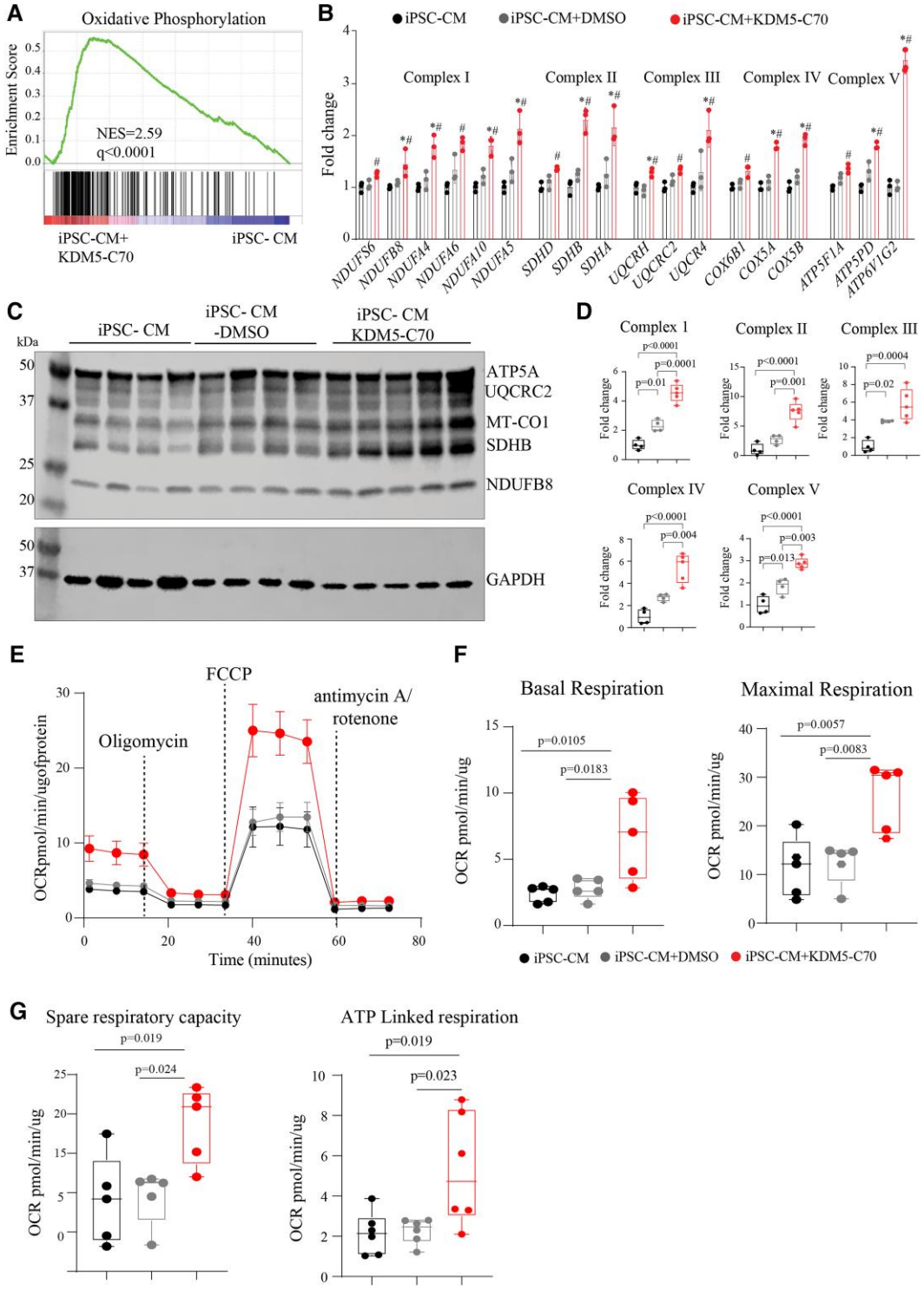

Figure 6 Effect of KDM5 inhibition on OXPHOS. (*A*) GSEA from DEGs-predicted activation of gene signature of OXPHOS upon KDM5 inhibition. (*B*) qPCR data showing transcript levels of selected OXPHOS genes from Complexes I to V. (*C* and *D*) Immunoblot analysis showing the expression of representative protein from Complexes I to V of the OXPHOS. (*E*) Panel shows kinetic data for real-time OCR measurements of hiPSC-CMs by Seahorse extracellular flux analyser in the controls and treated groups. Average data from 5 independent experiments each constituting an average of 10 wells/experiment is shown. Error bar indicates SEM. (*F* and *G*) KDM5-C70 treatment demonstrated a higher respiratory rate under baseline conditions and after mitochondrial decoupling. Quantitative data obtained from five independent experiments each constituting an average of 10 wells is shown. Pairwise corrected *P*-values after one-way ANOVA are shown.

maturation of iPSC-CM however complete functional maturation of these cells may require additional optimized substrates and stimuli to fully reprogramme these cells to a mature state. Finally, the individual contribution of each KDM5 to cardiac gene regulation remained unknown. Given that the KDM5s can compensate for the lack of each other such stuides will require extensive single and double deletion strain for KDM5. Future studies will be required to ascertain these individual and overlapping roles of KDM5 in CM homeostasis. Nonetheless, our data provide a first insight into the role of KDM5s in CMs and provide evidence that inhibition of KDM5 has a notable effect on the sarcomere, OXPHOS, and FAO genes that prime the iPSC-CMs towards maturation.

5. Conclusion

Overall, our data show the importance of KDM5 in regulating CM maturation and demonstrate its effect on OXPHOS and sarcomere gene regulation. Remarkably, KDM5 represses CM maturation and consequently reduces the expression of FAO and genes involved in sarcomere formation. Therefore, we conclude that KDM5 represents a novel target in the regulation of CM maturation and may have potent therapeutic effects in combination with other known myocyte maturation strategies.

Supplementary material

Supplementary material is available at *Cardiovascular Research* online.

Acknowledgements

We thank the MDACC Epigenomics Profiling Core Facility for their assistance with the CUT&RUN assays.

Conflict of interest: none declared

Funding

P.G. is supported by NHLBI (HL165334-01). A.J.M. is supported by the NHLBI (HL151737 and HL132401) and National institute of aging (NIA) (AG082751). This work was also supported by the Ewing Halsell Foundation (A.J.M.), John. Dunn foundation (P.G.). F.A. supported in part by grants from the NHLBI-R01HL158703 and the Houston Methodist Cornerstone Award. L.V.-Z. was supported by a predoctoral fellowship and travel scholarship from the Chilean National Agency for Research and Development (ANID 21200450).

Data availability

The data underlying this article are available in Gene Expression Omnibus (GEO) and can be accessed with GEO accession number GSE250210.

References

1. Bergmann O, Bhardwaj RD, Bernard S, Zdunek S, Barnabe-Heider F, Walsh S, Zupicich J, Alkass K, Buchholz BA, Druid H, Jovinge S, Frisen J. Evidence for cardiomyocyte renewal in humans. *Science* 2009;**324**:98–102.
2. Senyo SE, Steinhauser ML, Pizzimenti CL, Yang VK, Cai L, Wang M, Wu TD, Guerquin-Kern JL, Lechene CP, Lee RT. Mammalian heart renewal by pre-existing cardiomyocytes. *Nature* 2013;**493**:433–436.
3. Rubart M, Field LJ. Cardiac regeneration: repopulating the heart. *Annu Rev Physiol* 2006;**68**:29–49.
4. Yuan X, Braun T. Multimodal regulation of cardiac myocyte proliferation. *Circ Res* 2017;**121**:293–309.
5. Porrello ER, Mahmoud AI, Simpson E, Hill JA, Richardson JA, Olson EN, Sadek HA. Transient regenerative potential of the neonatal mouse heart. *Science* 2011;**331**:1078–1080.
6. Guo Y, Pu WT. Cardiomyocyte maturation: new phase in development. *Circ Res* 2020;**126**:1086–1106.
7. Karbassi E, Fenix A, Marchiano S, Muraoka N, Nakamura K, Yang X, Murry CE. Cardiomyocyte maturation: advances in knowledge and implications for regenerative medicine. *Nat Rev Cardiol* 2020;**17**:341–359.
8. Uosaki H, Cahan P, Lee DI, Wang S, Miyamoto M, Fernandez L, Kass DA, Kwon C. Transcriptional landscape of cardiomyocyte maturation. *Cell Rep* 2015;**13**:1705–1716.
9. Tu C, Mezynski R, Wu JC. Improving the engraftment and integration of cell transplantation for cardiac regeneration. *Cardiovasc Res* 2020;**116**:473–475.
10. Tu C, Chao BS, Wu JC. Strategies for improving the maturity of human induced pluripotent stem cell-derived cardiomyocytes. *Circ Res* 2018;**123**:512–514.
11. Yang X, Pabon L, Murry CE. Engineering adolescence: maturation of human pluripotent stem cell-derived cardiomyocytes. *Circ Res* 2014;**114**:511–523.
12. Liu YW, Chen B, Yang X, Fugate JA, Kalucki FA, Futakuchi-Tsuchida A, Couture L, Vogel KW, Astley CA, Baldessari A, Ogle J, Don CW, Steinberg ZL, Seslar SP, Tuck SA, Tsuchida H, Naumova AV, Dupras SK, Lyu MS, Lee J, Hailey DW, Reinecke H, Pabon L, Fryer BH, MacLellan WR, Thies RS, Murry CE. Human embryonic stem cell-derived cardiomyocytes restore function in infarcted hearts of non-human primates. *Nat Biotechnol* 2018;**36**:597–605.
13. Auguste G, Rouhi L, Matkovich SJ, Coarfa C, Robertson MJ, Czernuszewicz G, Gurha P, Marian AJ. BET bromodomain inhibition attenuates cardiac phenotype in myocyte-specific lamin A/C-deficient mice. *J Clin Invest* 2020;**130**:4740–4758.
14. Gilsbach R, Preissl S, Gruning BA, Schnick T, Burger L, Benes V, Wurch A, Bonisch U, Gunther S, Backofen R, Fleischmann BK, Schubeler D, Hein L. Dynamic DNA methylation orchestrates cardiomyocyte development, maturation and disease. *Nat Commun* 2014;**5**:5288.
15. Papait R, Cattaneo P, Kunderfranco P, Greco C, Carullo P, Guffanti A, Viganò V, Stirparo GG, Latronico MV, Hasenfuss G, Chen J, Condorelli G. Genome-wide analysis of histone marks identifying an epigenetic signature of promoters and enhancers underlying cardiac hypertrophy. *Proc Natl Acad Sci U S A* 2013;**110**:20164–20169.
16. Coste Pradas J, Auguste G, Matkovich SJ, Lombardi R, Chen SN, Garnett T, Chamberlain K, Riyad JM, Weber T, Singh SK, Robertson MJ, Coarfa C, Marian AJ, Gurha P. Identification of genes and pathways regulated by lamin A in heart. *J Am Heart Assoc* 2020;**9**:e015690.
17. Ruthenburg AJ, Allis CD, Wysocka J. Methylation of lysine 4 on histone H3: intricacy of writing and reading a single epigenetic mark. *Mol Cell* 2007;**25**:15–30.
18. Liu X, Secombe J. The histone demethylase KDM5 activates gene expression by recognizing chromatin context through its PHD reader motif. *Cell Rep* 2015;**13**:2219–2231.
19. Lussi YC, Mariani L, Friis C, Peltonen J, Myers TR, Krag C, Wong G, Salcini AE. Impaired removal of H3K4 methylation affects cell fate determination and gene transcription. *Development* 2016;**143**:3751–3762.
20. Gerbin KA, Grancharova T, Donovan-Maiye RM, Hendershott MC, Anderson HG, Brown JM, Chen J, Dinh SQ, Gehring JL, Johnson GR, Lee H, Nath A, Nelson AM, Sluzewski MF, Viana MP, Yan C, Zaunbrecher RJ, Cordes Metzler KR, Gaudreault N, Knijnenburg TA, Rafelski SM, Theriot JA, Gunawardane RN. Cell states beyond transcriptomics: integrating structural organization and gene expression in hiPSC-derived cardiomyocytes. *Cell Syst* 2021;**12**:670–687.e10.
21. Grancharova T, Gerbin KA, Rosenberg AB, Roco CM, Arakaki JE, DeLizo CM, Dinh SQ, Donovan-Maiye RM, Hirano M, Nelson AM, Tang J, Theriot JA, Yan C, Menon V, Palecek SP, Seelig G, Gunawardane RN. A comprehensive analysis of gene expression changes in a high replicate and open-source dataset of differentiating hiPSC-derived cardiomyocytes. *Sci Rep* 2021;**11**:15845.
22. Lian X, Zhang J, Azarin SM, Zhu K, Hazeltine LB, Bao X, Hsiao C, Kamp TJ, Palecek SP. Directed cardiomyocyte differentiation from human pluripotent stem cells by modulating Wnt/beta-catenin signaling under fully defined conditions. *Nat Protoc* 2013;**8**:162–175.
23. Burridge PW, Matsa E, Shukla P, Lin ZC, Churko JM, Ebert AD, Lan F, Diecke S, Huber B, Mordwinkin NM, Plews JR, Abilez OJ, Cui B, Gold JD, Wu JC. Chemically defined generation of human cardiomyocytes. *Nat Methods* 2014;**11**:855–860.
24. Horton JR, Liu X, Gale M, Wu L, Shanks JR, Zhang X, Webber PJ, Bell JSK, Kales SC, Mott BT, Rai G, Jansen DJ, Henderson MJ, Urban DJ, Hall MD, Simeonov A, Maloney DJ, Johns MA, Fu H, Jadhav A, Vertino PM, Yan Q, Cheng X. Structural basis for KDM5A histone lysine demethylase inhibition by diverse compounds. *Cell Chem Biol* 2016;**23**:769–781.
25. Johansson C, Velupillai S, Tumber A, Szykowska A, Hookway ES, Nowak RP, Strain-Damerell C, Gileadi C, Philpott M, Burgess-Brown N, Wu N, Kopec J, Nuzzi A, Steuber H, Egner U, Badock V, Munro S, LaThangue NB, Westaway S, Brown J, Athanasou N, Prinjha R, Brennan PE, Oppermann U. Structural analysis of human KDM5B guides histone demethylase inhibitor development. *Nat Chem Biol* 2016;**12**:539–545.
26. Lee HR, Ann J, Kim YM, Lee J, Kim HJ. The KDM5 inhibitor KDM5-C70 induces astrocyte differentiation in rat neural stem cells. *ACS Chem Neurosci* 2021;**12**:441–446.
27. Gurha P, Chen X, Lombardi R, Willerson JT, Marian AJ. Knockdown of plakophilin 2 downregulates miR-184 through CpG hypermethylation and suppression of the E2F1 pathway and leads to enhanced adipogenesis in vitro. *Circ Res* 2016;**119**:731–750.
28. Auguste G, Gurha P, Lombardi R, Coarfa C, Willerson JT, Marian AJ. Suppression of activated FOXO transcription factors in the heart prolongs survival in a mouse model of laminopathies. *Circ Res* 2018;**122**:678–692.
29. Olcum M, Cheedipudi SM, Rouhi L, Fan S, Jeong HH, Zhao Z, Gurha P, Marian AJ. The WNT/beta-catenin pathway regulates expression of the genes involved in cell cycle progression and mitochondrial oxidative phosphorylation in the postmitotic cardiac myocytes. *J Cardiovasc Aging* 2022;**2**:15.
30. Liao Y, Smyth GK, Shi W. featureCounts: an efficient general purpose program for assigning sequence reads to genomic features. *Bioinformatics* 2014;**30**:923–930.
31. Dobin A, Davis CA, Schlesinger F, Drenkow J, Zaleski C, Jha S, Batut P, Chaisson M, Gingeras TR. STAR: ultrafast universal RNA-seq aligner. *Bioinformatics* 2013;**29**:15–21.
32. Law CW, Chen Y, Shi W, Smyth GK. Voom: precision weights unlock linear model analysis tools for RNA-seq read counts. *Genome Biol* 2014;**15**:R29.

33. Skene PJ, Henikoff S. An efficient targeted nuclease strategy for high-resolution mapping of DNA binding sites. *Elife* 2017;**6**:e21856.
34. Meers MP, Tenenbaum D, Henikoff S. Peak calling by Sparse Enrichment Analysis for CUT&RUN chromatin profiling. *Epigenetics Chromatin* 2019;**12**:42.
35. Meers MP, Bryson TD, Henikoff JG, Henikoff S. Improved CUT&RUN chromatin profiling tools. *Elife* 2019;**8**:e46314.
36. Sakamoto T, Matsuura TR, Wan S, Ryba DM, Kim JU, Won KJ, Lai L, Petucci C, Petrenko N, Musunuru K, Vega RB, Kelly DP. A critical role for estrogen-related receptor signaling in cardiac maturation. *Circ Res* 2020;**126**:1685–1702.
37. Yang D, Gomez-Garcia J, Funakoshi S, Tran T, Fernandes I, Bader GD, Laflamme MA, Keller GM. Modeling human multi-lineage heart field development with pluripotent stem cells. *Cell Stem Cell* 2022;**29**:1382–1401.e8.
38. Funakoshi S, Fernandes I, Mastikhina O, Wilkinson D, Tran T, Dhahri W, Mazine A, Yang D, Burnett B, Lee J, Protze S, Bader GD, Nunes SS, Laflamme M, Keller G. Generation of mature compact ventricular cardiomyocytes from human pluripotent stem cells. *Nat Commun* 2021;**12**:3155.
39. Garbern JC, Helman A, Sereda R, Sarikhani M, Ahmed A, Escalante GO, Ogurlu R, Kim SL, Zimmerman JF, Cho A, MacQueen L, Bezzerides VJ, Parker KK, Melton DA, Lee RT. Inhibition of mTOR signaling enhances maturation of cardiomyocytes derived from human-induced pluripotent stem cells via p53-induced quiescence. *Circulation* 2020;**141**:285–300.
40. Herron TJ, Rocha AM, Campbell KF, Ponce-Balbuena D, Willis BC, Guerrero-Serna G, Liu Q, Klos M, Musa H, Zarzoso M, Bizy A, Furness J, Anumonwo J, Mironov S, Jalife J. Extracellular matrix-mediated maturation of human pluripotent stem cell-derived cardiac monolayer structure and electrophysiological function. *Circ Arrhythm Electrophysiol* 2016;**9**:e003638.
41. Dhahri W, Sadikov Valdman T, Wilkinson D, Pereira E, Ceylan E, Andharia N, Qiang B, Masoudpour H, Wulkan F, Quesnel E, Jiang W, Funakoshi S, Mazine A, Gomez-Garcia MJ, Latifi N, Jiang Y, Huszti E, Simmons CA, Keller G, Laflamme MA. In vitro matured human pluripotent stem cell-derived cardiomyocytes form grafts with enhanced structure and function in injured hearts. *Circulation* 2022;**145**:1412–1426.
42. Lopaschuk GD, Karwi QG, Tian R, Wende AR, Abel ED. Cardiac energy metabolism in heart failure. *Circ Res* 2021;**128**:1487–1513.
43. Beshiri ML, Holmes KB, Richter WF, Hess S, Islam AB, Yan Q, Plante L, Litovchick L, Gévry N, Lopez-Bigas N, Kaelin WG, Benevolenskaya EV. Coordinated repression of cell cycle genes by KDM5A and E2F4 during differentiation. *Proc Natl Acad Sci U S A* 2012;**109**:18499–18504.
44. Liefke R, Oswald F, Alvarado C, Ferres-Marco D, Mittler G, Rodriguez P, Dominguez M, Borggrefe T. Histone demethylase KDM5A is an integral part of the core Notch-RBP-J repressor complex. *Genes Dev* 2010;**24**:590–601.
45. Wong PP, Miranda F, Chan KV, Berlato C, Hurst HC, Scibetta AG. Histone demethylase KDM5B collaborates with TFAP2C and Myc to repress the cell cycle inhibitor p21(cip) (CDKN1A). *Mol Cell Biol* 2012;**32**:1633–1644.
46. Wang B, Tan Y, Zhang Y, Zhang S, Duan X, Jiang Y, Li T, Zhou Q, Liu X, Zhan Z. Loss of KDM5B ameliorates pathological cardiac fibrosis and dysfunction by epigenetically enhancing ATF3 expression. *Exp Mol Med* 2022;**54**:2175–2187.
47. Cui J, Quan M, Xie D, Gao Y, Guha S, Fallon MB, Chen J, Xie K. A novel KDM5A/MPC-1 signaling pathway promotes pancreatic cancer progression via redirecting mitochondrial pyruvate metabolism. *Oncogene* 2020;**39**:1140–1151.
48. Wang T, McDonald C, Petrenko NB, Leblanc M, Wang T, Giguere V, Evans RM, Patel VV, Pei L. Estrogen-related receptor alpha (ERRalpha) and ERRgamma are essential coordinators of cardiac metabolism and function. *Mol Cell Biol* 2015;**35**:1281–1298.
49. Miki K, Deguchi K, Nakanishi-Koakutsu M, Lucena-Cacace A, Kondo S, Fujiwara Y, Hatani T, Sasaki M, Naka Y, Okubo C, Narita M, Takei I, Napier SC, Sugo T, Imaichi S, Monjo T, Ando T, Tamura N, Imahashi K, Nishimoto T, Yoshida Y. ERRγ enhances cardiac maturation with T-tubule formation in human iPSC-derived cardiomyocytes. *Nat Commun* 2021;**12**:3596.
50. Sakamoto T, Batmanov K, Wan S, Guo Y, Lai L, Vega RB, Kelly DP. The nuclear receptor ERR cooperates with the cardiogenic factor GATA4 to orchestrate cardiomyocyte maturation. *Nat Commun* 2022;**13**:1991.
51. Wang H, Fan Z, Shliaha PV, Miele M, Hendrickson RC, Jiang X, Helin K. H3k4me3 regulates RNA polymerase II promoter-proximal pause-release. *Nature* 2023;**615**:339–348.